cAMP activation of PKA defines an ancient signaling mechanism

Rahul Das*, Veronica Esposito*, Mona Abu-Abed*, Ganesh S. Anand†, Susan S. Taylor†‡, and Giuseppe Melacini*‡

*Departments of Chemistry, Biochemistry, and Biomedical Sciences, McMaster University, 1280 Main Street West, Hamilton, ON, Canada L8S 4M1; and †Department of Chemistry and Biochemistry, Howard Hughes Medical Institute, Department of Pharmacology, University of California at San Diego, 9500 Gilman Drive, La Jolla, CA 92093

Contributed by Susan S. Taylor, October 16, 2006 (sent for review September 20, 2006)

cAMP and the cAMP binding domain (CBD) constitute a ubiquitous regulatory switch that translates an extracellular signal into a biological response. The CBD contains α- and β-subdomains with cAMP binding to a phosphate binding cassette (PBC) in the β-sandwich. The major receptors for cAMP in mammalian cells are the regulatory subunits (R-subunits) of PKA where cAMP and the catalytic subunit compete for the same CBD. The R-subunits inhibit kinase activity, whereas cAMP releases that inhibition. Here, we use NMR to map at residue resolution the cAMP-dependent interaction network of the CBD-A domain of isoform Iα of the R-subunit of PKA. Based on H/D, H/H, and N_z exchange data, we propose a molecular model for the allosteric regulation of PKA by cAMP. According to our model, cAMP binding causes long-range perturbations that propagate well beyond the immediate surroundings of the PBC and involve two key relay sites located at the C terminus of β_2 (I163) and N terminus of β_3 (D170). The I163 site functions as one of the key triggers of global unfolding, whereas the D170 locus acts as an electrostatic switch that mediates the communication between the PBC and the B-helix. Removal of cAMP not only disrupts the cap for the B′ helix within the PBC, but also breaks the circuitry of cooperative interactions stemming from the PBC, thereby uncoupling the α- and β-subdomains. The proposed model defines a signaling mechanism, conserved in every genome, where allosteric binding of a small ligand disrupts a large protein–protein interface.

allostery | NMR | cyclic nucleotide binding domain

The cAMP binding domain (CBD) and cAMP are conserved from bacteria to humans as a ubiquitous signaling mechanism to translate extracellular stress signals into appropriate biological responses (1). The major receptor for cAMP in higher eukaryotes, cAMP-dependent PKA (2), is ubiquitous in mammalian cells where it exists in two forms: the inactive tetrameric holoenzyme and the active dissociated catalytic subunit (C-subunit). In the inactive holoenzyme, two C-subunits are bound to a dimeric regulatory subunit (R-subunit) (Fig. 1*a*). Upon binding cAMP, the R-subunits undergo a conformational change that unleashes the active C-subunits (3, 4). The R-subunits are composed of an N-terminal dimerization/docking domain, a flexible linker that includes an autoinhibitory segment, and two tandem CBDs (CBD-A and CBD-B; Fig. 1*b*) (5). The CBD-A of the isoform Iα of the R-subunit of PKA (RIα) contains a noncontiguous α-subdomain, which mediates the interactions with the C-subunit and a contiguous β-subdomain that forms a β-sandwich and contains the cAMP binding pocket (i.e., the phosphate binding cassette or PBC) (Fig. 1 *c* and *d*) (6).

Crystal structures of CBD-A of RIα in its cAMP- (6) and C-bound (7) states have revealed two very different conformations, highlighting the conformational plasticity of this ancient domain. Although these static crystal structures define two stable end points, questions remain about the allosteric control of the reversible shuttling between the two states. How does the signal generated by cAMP binding to the PBC (Fig. 1 *c* and *d*) propagate through a long-range allosteric network that spans both α- and β-subdomains? Previous analyses (8–16) have led to the proposal of an initial allosteric model in which the α- and β-subdomains are directly coupled to each other through a salt bridge between E200 and R241 and also possibly through a hydrophobic hinge defined by the L203, I204, and Y229 side-chain cluster (9, 11, 12). However, mutations (17), sequence conservation analyses (1), structure-based comparisons (1), and genetic screening (18, 19) indicate that several other sites, which are not accounted for by the existing model, are also likely to play an active role in the cAMP-mediated activation of PKA. To comprehensively understand this allosteric mechanism, it is therefore necessary to elucidate at high resolution how cAMP remodels the free energy landscape of CBD-A, which serves as the central controlling unit of PKA. For this purpose, we have investigated by NMR RIα (residues 119–244), a construct that spans both α- and β-subdomains of CBD-A and retains high-

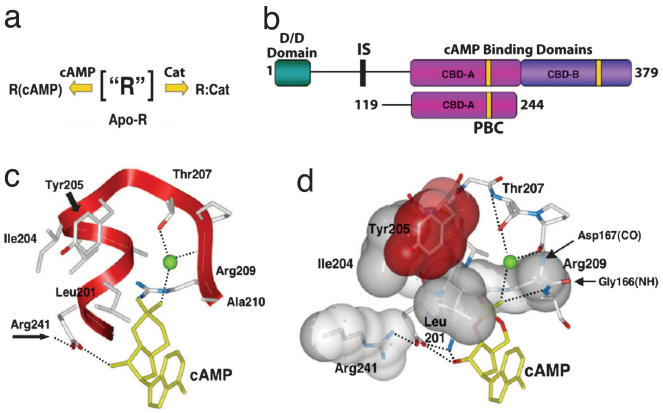

Fig. 1. Domain organization of RIα and the PBC. (*a*) Possible states for the R-subunit. (*b*) Schematic representation of the domain organization in R. The line connecting the dimerization/docking domain (turquoise) to the CBD-A (magenta) represents the flexible linker region. The PBCs are yellow; CBD-B is purple. Also indicated is a schematic diagram for the RIα (residues 119–244) construct studied here. (*c*) The PBC (residues 199–210) for CBD-A of RIα and selected interactions with cAMP. The green ball denotes a bound water molecule. (*d*) The hydrophobic shell of the PBC is based on the 1RGS coordinates (6).

Author contributions: S.S.T. and G.M. designed research; R.D. and G.M. performed research; G.S.A. and S.S.T. contributed new reagents/analytic tools; R.D., V.E., M.A.-A., and G.M. analyzed data; and G.M. wrote the paper.

The authors declare no conflict of interest.

Abbreviations: C-subunit, catalytic subunit; CBD, cAMP-binding domain; HSQC, heteronuclear single-quantum coherence; PBC, phosphate binding cassette; PF, protection factor; R-subunit, regulatory subunit; RIα, isoform Iα of the R-subunit of PKA; SASA, solvent-accessible surface area.

Data deposition: The NMR chemical shifts have been deposited in the BioMagResBank, www.bmrb.wisc.edu (accession no. 6984).

‡To whom correspondence may be addressed. E-mail: melacin@mcmaster.ca or staylor@ucsd.edu.

This article contains supporting information online at www.pnas.org/cgi/content/full/0609033103/DC1.

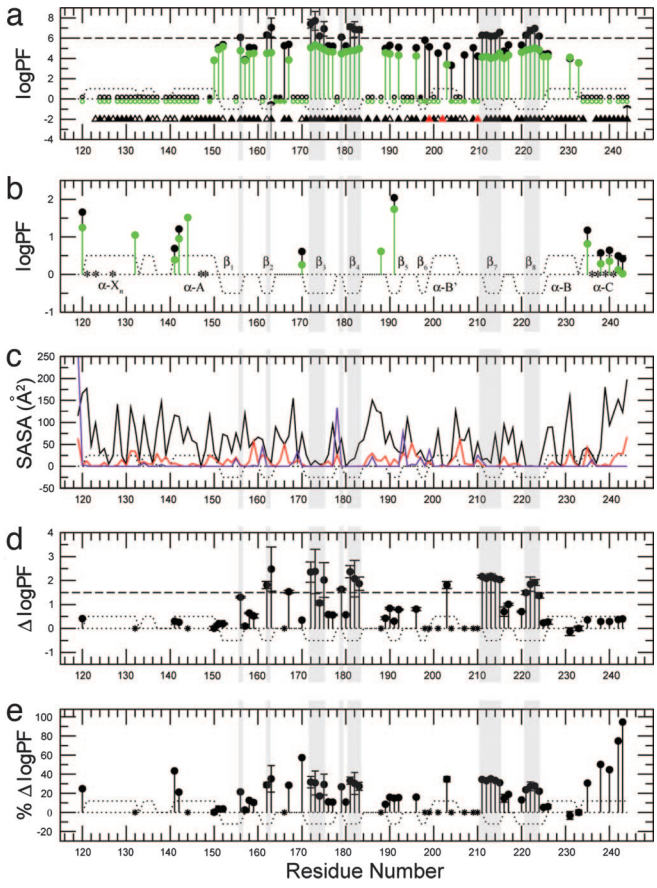

Fig. 2. PFs of RIα (residues 119–244) based on H/D and H/H exchange. (*a*) PFs derived from H/D exchange rates measured for RIα (residues 119–244) with (black) and without (green) 10-fold excess cAMP at 306 K and in 50 mM Mes (pH 6.5)/100 mM NaCl/0.02% NaN_3. Filled circles indicate amide protons that exchange slowly enough to enable the measurement of quantitative H/D exchange rates; empty circles denote amide protons that were fully exchanged within the dead time of the experiment (≈20 min); stars indicate amide protons that could be detected only in the first HSQC spectrum acquired after exposure to D_2O, but not in the subsequent spectra. The triangles indicate the presence of hydrogen bonds donated by the backbone amide hydrogen. Filled triangles indicate hydrogen bonds with H—O distance <2.40 Å and H-N . . . O angle <35°, and open triangles indicate hydrogen bonds fulfilling less severe geometric criteria (H—O distance <2.85 Å and H-N . . . O angle <47°). Red triangles represent intermolecular (protein-cAMP) hydrogen bonds. The arrow at I163 signifies that for this residue no significant HSQC intensity change was observed during the course of the H/D experiment and therefore the reported PF value should just be interpreted as a PF lower limit. The arrow at Y244 means that for this residue a bimodal behavior is observed in the presence of 10-fold excess cAMP: whereas most of the Y244 HSQC cross-peak intensity is lost in the first HSQC spectrum, a small but detectable residual signal remains until the completion of the H/D experiment. Residues for which no symbol is reported are ambiguous because of overlap or are prolines (P153 and P208). (*b*) PFs derived from H/H exchange rates measured under the same conditions reported for *a*. The green/black color coding is the same as in *a*. Residues 132, 144, and 188 exchange fast enough to result in detectable H/H exchange CLEANEX cross-peaks only in the absence of cAMP excess (green). Residues marked with a star could not be unambiguously assigned in the CLEANEX spectrum because of overlap. (*c*) Residue-specific SASAs for the bound form. The black solid line indicates the total (backbone and side-chain) SASAs, and the red line refers to the backbone-only SASAs. The violet line refers to SASAs for backbone N atoms scaled up by a factor of 10. The reported SASA values should be considered as upper limits because the shielding effect of tightly bound water molecules and cAMP is not accounted for. (*d*) Differences between the PF logarithms measured with and without cAMP excess, shown in *a* and *b* in black and green, respectively. (e) As in *d*, but showing the effect of cAMP excess removal as percentage variations in PF logarithms (i.e., $100 \times \Delta\text{logPF}/\text{logPF}_{\text{bound}}$). In all images, dotted lines represent the secondary structure expected for RIα (residues 119–244) based on the coordinates of the cAMP-bound R-subunit (6). Positive dots indicate α-helices or turns, and negative dots denote β-strands. Gray shading indicates residues with $\log_{10}(\text{PF}) > 6$ in the cAMP bound form, i.e., class *c* residues. In *d* and *e* stars denote residues that exchange too fast in the absence of excess cAMP for a quantitative PF determination by H/D exchange or too slow in the presence of bound cAMP for the detection of H/H exchange cross-peaks.

affinity binding to cAMP. Based on the Cα and Cβ ppm values this RIα segment preserves a very similar fold to that observed in a longer R fragment spanning both tandem CBDs (6) [see supporting information (SI) Fig. 5], verifying that RIα (residues 119–244) represents a good model for CBD-A.

Using a combined NMR approach based on H/D and H/H exchange (Fig. 2) and chemical-shift changes measured through N_Z-exchange spectroscopy (Fig. 3) we have mapped at residue resolution the interaction networks that propagate the cAMP signal within CBD-A. Our results define an allosteric model (Fig. 4) according to which cAMP release breaks a long-range circuitry uncoupling the α- and β-subdomains and thereby unleashing distal "hot spots" that serve as primary interaction sites for recognition of the C-subunit. Our findings reported here are a successful attempt of studying CBD-A of the R-subunit by multidimensional solution NMR methods. Furthermore, the proposed model defines a mechanism that is highly conserved and thus relevant for cAMP recognition in other homologous CBDs coupled to effector proteins with diverse functions, such as transcription factors (catabolite-activator protein) (20–31), guanine nucleotide exchange factors (11), and ion channel proteins (both hyperpolarization-activated cyclic nucleotide-dependent channels and cyclic nucleotide-gated channels) (32, 33). This model also serves as a general paradigm for how small molecules such as cAMP allosterically control large protein–protein interfaces.

Results and Discussion

cAMP Binding Affects All of the CBD-A Sites Directly or Indirectly Involved in C Recognition and Causes Decreased Solvent Exposure. The protection factors (PFs) based on the H/D and H/H exchange rates measured before and after excess cAMP was dialyzed out, are reported in Fig. 2 *a* and *b*, respectively. The corresponding absolute and percentage differences in the logPFs are shown in Fig. 2 *d* and *e*, respectively. The first key feature that emerges from Fig. 2*a* is the dramatic decrease in protection upon removal of excess cAMP for most of the residues within the PBC. Interestingly, a marked decrease in solvent exposure is observed not only for amide sites that are directly hydrogen-bonded to cAMP, such as G199 and A210 (Fig. 2*a* and SI Table 1), but also for the other amides in the PBC. Indeed, when cAMP levels are substoichiometric, the entire PBC with the exception of L203 exchanges more rapidly with the bulk solvent. This behavior is explained considering that removal of cAMP most notably removes the N-terminal capping mechanism for the PBC's B′ helix (6), which is therefore destabilized. The B′ helix is one of the R:C interaction sites and includes Y205, which nucleates a major hydrophobic interface between the R- and C-subunits (7). By releasing the helix cap generated through the cyclic phosphate, the removal of cAMP now frees up this tip of the PBC so that it is available to dock to the C-subunit. The PF variations within the PBC therefore provide an initial understanding of a first level of cAMP control for the R:C interactions.

An additional level of cAMP control for the R:C interactions is revealed by Fig. 2*b*, which shows that cAMP removal results in increased solvent exposure also at several other R:C contact sites well outside of the immediate PBC, consistently with the existence of a long-range interaction network nucleated by the docking of cAMP and impaired by the elimination of cAMP. For instance, the H/H-based PFs (Fig. 2 *b* and *e*) clearly indicate that cAMP-release enhances the solvent exposure of both the X_N/A-helix loop and the C-helix. These two motifs are both essential

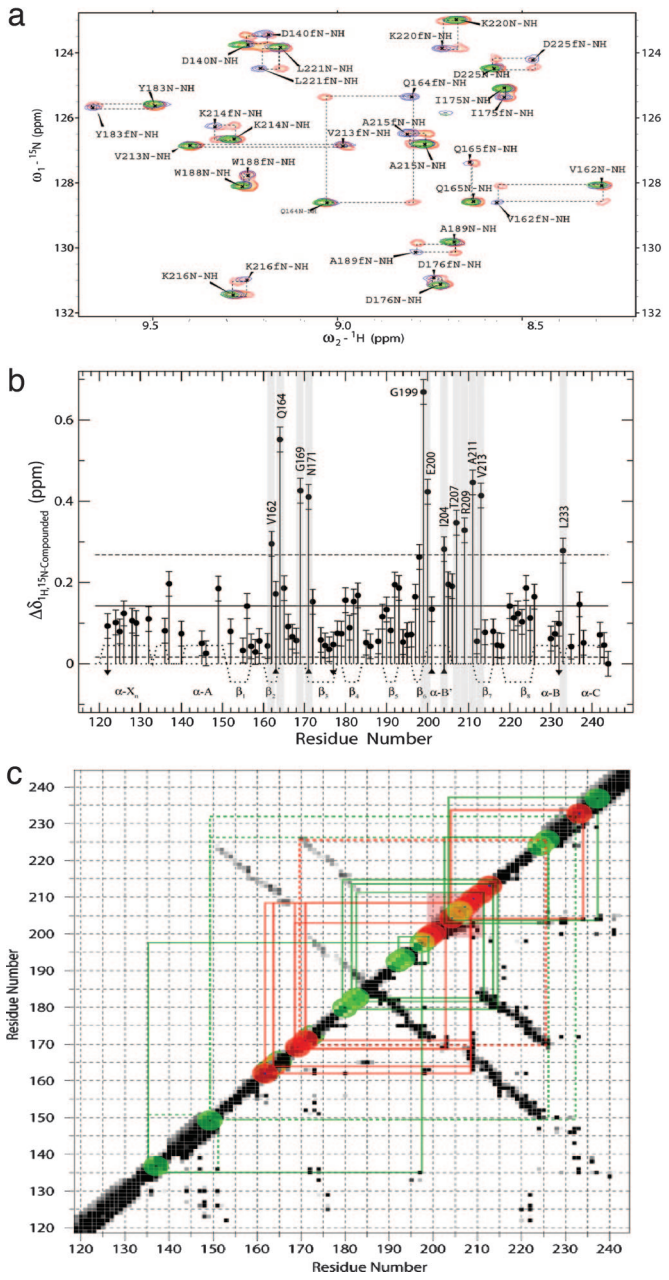

Fig. 3. Effect of cAMP on RIα (residues 119–244) based on chemical-shift changes. (*a*) Representative expansion of the N_z-exchange spectrum (orange) overlaid to the HSQC spectra of cAMP-free (blue) and cAMP-bound (green) RIα (residues 119–244). Dashed boxes highlight the N_z exchange cross-peaks that correlate the free and bound states. Labels indicate cross-peak assignments, and f denotes the assignments of the free form. (*b*) Plot of the compounded ^1H,^{15}N chemical-shift changes vs. residue number. The solid and dashed horizontal lines mark the average compounded ^1H,^{15}N chemical shift ± SD, respectively. Residues for which the observed compounded ^1H,^{15}N chemical shift is larger than the average + SD (i.e., ''hot spots'') are highlighted with a gray background. Down/up arrows indicate that the reported compounded ppm change is only an upper/lower limit, respectively, because of either spectral overlap or the assignment of only one N_z exchange cross-peak. Residues for which no data are shown are ambiguous or are prolines (P153 and P208). The secondary structure is reported as in Fig. 2. (*c*) Contact map for RIα (residues 119–244) overlaid to the sites with the most significant compounded chemical-shift changes. A black (white) pixel is shown for a given residue pair if the minimum distance between two atoms of these two residues is <3 Å (>5 Å). For all other cases the color of the pixel is interpolated within a gray scale. In the upper left side of the diagonal only backbone-to-backbone distances are shown, whereas in the lower right side of the diagonal all distances are considered. The α-helices are clustered along the diagonal, whereas the β-strands contacts within the β-barrel are represented by the two antidiagonals. The red transparent square indicates the PBC, and the red dots along the diagonal correspond to sites with compounded ^1H,^{15}N chemical shift > average + 1 SD. The green dots indicate regions with compounded ^1H,^{15}N chemical shift between the average + 1 SD and the average. The size of the red and green dots takes into account that chemical-shift changes report on perturbations not only in the residue for which the change is observed but also in its proximity. The red (green) solid lines connect the red (green) sites to the PBC or neighboring residues through direct interresidue contacts. The dashed lines indicate selected contacts that are not directly involved with the PBC.

elements for docking R to C in the holoenzyme complex (7), and the cAMP-induced long-range perturbations at these sites are in agreement with the observed cAMP-dependent chemical shift variations (Fig. 3). These observations provide therefore experimental proof of the importance of allosteric mechanisms that couple the PBC and the C-helix, such as the E200/R241 salt bridge (9) and the hydrophobic hinge (11, 12).

Fig. 2 *b* and *e* also reveals that other significant cAMP-induced changes in solvent shielding occur at sites not directly involved in R:C interactions. For instance, the maps of both the H/H-based PF variations (Fig. 2*e*) and the chemical-shift changes (Fig. 3*b*) point to a major cAMP effect on the locus centered at D170 and located at the N terminus of β_3. This region is not involved in direct interactions with the C-subunit of PKA; however, at this site significant local conformational changes are observed upon C-subunit binding at both the level of backbone local RMSD (SI Fig. 6) and side-chain orientation, with the D170 χ_1 dihedral angle changing from 48° in the cAMP-bound to −107° in the C-bound states of CBD-A (Fig. 4 *e* and *f*) (6, 7). This correlation between C binding and the conformation of D170 suggests that the D170 region may serve as an additional site available for cAMP to control C recognition by R. Another region of CBD-A, which is not directly involved in C binding but for which the local conformation is indirectly affected by C, is the C terminus of the X_N-helix (SI Fig. 6). Similarly to D170, the H/H-based PF maps (Fig. 2 *b* and *e*) point to a decrease in solvent shielding upon cAMP release also at this site. Therefore, this locus may also offer further opportunities for controlling the R:C recognition by cAMP.

H/D Exchange of the β-Subdomain Inner Core Amides Is Concertedly Controlled by Transient Global Unfolding Events and Is Highly cAMP-Sensitive. Another remarkable feature of the PF variations reported in Fig. 2*d* is that the most dramatic quantifiable absolute PF changes occurring upon cAMP excess removal match quite well with those residues characterized by high PFs in the cAMP-bound form ($\log_{10}PF_{cAMP\text{-}Bound} > 6$; Fig. 2*a*). This class of highly protected core residues is confined exclusively within the CBD-A β-subdomain, in marked contrast with the α-subdomain in which most of the residues exchange rapidly with the solvent (Fig. 2*a*). Within the β-subdomain, the residues with $\log PF_{cAMP\text{-}Bound} > 6$ map well to the C terminus of strands $\beta_{1,2}$ and most of the amides in the β-barrel inner strands β_{3-4} and β_{7-8} (Fig. 2*a*), which in turn match well with local minima of the solvent-accessible surface area (SASA) plot (Fig. 2*c*). Consistently with the deep burial within the protein of these core amides with $\log PF_{cAMP\text{-}Bound} > 6$ (Fig. 2 *a* and *c*), it has been previously reported that the exchange pathways for the residues with maximal PFs often require transient global unfolding (34–36). To verify whether this result applies also to our system we calculated the average free energy change of the opening transition to exchange-competent states ($\Delta G_{opening}$) for the residues with $\log PF_{cAMP\text{-}Bound} > 6$ and then we compared it to that of global unfolding ($\Delta G_{unfolding}$) measured independently by urea denaturation of the cAMP-bound form (14, 37).

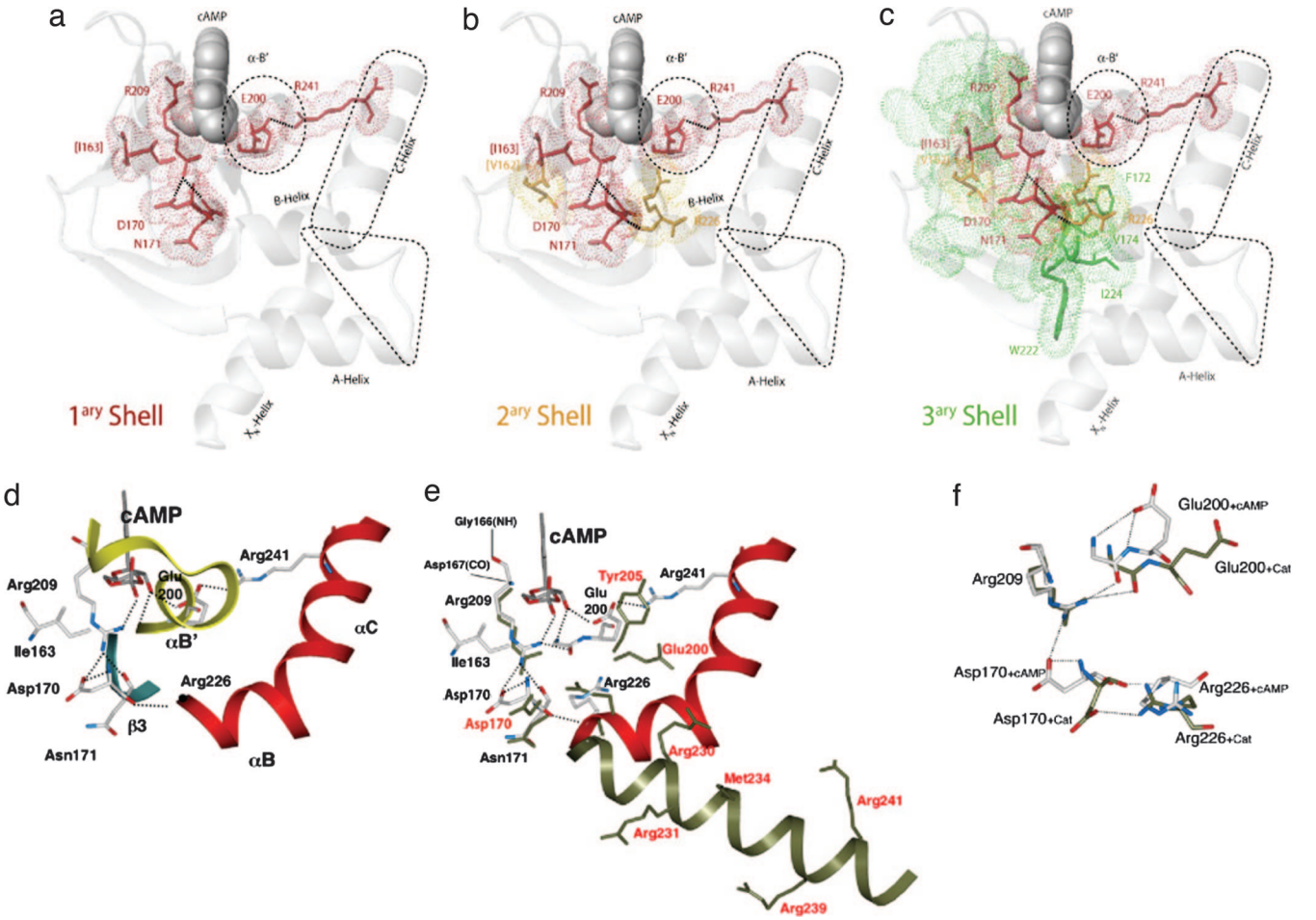

Fig. 4. Intramolecular signaling networks that propagate the cAMP signal from the PBC to the sites of C recognition. (*a–c*) Displayed is the progression from the first to the third contact shell residues, respectively, as explained in the text. Amino acids in the PBC or directly contacting it (first shell) are shown in red, those in the second shell are in orange, and those in the third shell are in green. For first- and second-shell residues bonds and van der Waals surfaces are displayed, and for third-shell residues detailed bonds are shown only if they are at the interface between the α- and the β-subdomains. Selected hydrogen bonds and salt bridges are indicated by thick dotted lines and regions that interface with the C-subunit are defined by dashed contours. Selected secondary structure elements and residues are labeled. Residue labels match the color of the contact shell to which they belong. Residue labels in parentheses are only hypothetical relay sites, as discussed in the text. All figures were created with the program MOLMOL (41) and atomic coordinates from the Protein Data Bank entry 1RGS (6). (*d–f*) The interactions of the primary shell are correlated with the conformational changes that are induced by the binding of the C-subunit. (*d*) The interactions that are favored in the cAMP-bound conformation are shown. The B/C helix is shown as a red ribbon. Highlighted are the ''electrostatic switches'' (D170 and R241) that, respectively, anchor β_3 and the C-helix to the PBC, whereas I163 shields the methylenes of R209. (*e*) Similar to *d* with the C-bound conformation (dark green) overlapped with the cAMP-bound conformation. (*f*) The changes in the positions of D170 and E200 in the two conformational states are highlighted.

For the $\Delta G_{\text{opening}}$ computation, we considered that unfolding of the R-subunit has been previously adequately described by using a two-state model (14) and that at pH 6.5 an EX2 Linderstrøm-Lang mechanism generally applies (36, 38). As a result, the average PF for residues with $\log PF_{\text{cAMP-Bound}} > 6$ (i.e., 6.6 ± 0.5) leads to a $\Delta G_{\text{opening}}$ of $\approx RT\ln(10^{6.6 \pm 0.5}) = 9.2 \pm 0.7$ kcal/mol. This $\Delta G_{\text{opening}}$ estimation is in good agreement with the $\Delta G_{\text{unfolding}}$ values measured independently by urea denaturation for cAMP-bound RIα (residues 119–244) (i.e., 10.1 ± 0.5 kcal/mol) and also for other related R-subunit constructs in the presence of excess cAMP (i.e., 9.2 ± 0.2 kcal/mol) (14, 37), further corroborating that global unfolding controls the opening transitions underlying the exchange behavior of residues with $\log PF_{\text{cAMP-Bound}} > 6$. This group of amino acids will be denoted here as ''class *c*'' residues, where *c* refers to their *c*oncerted exchange behavior ensuing from transient global unfolding events. Given the collective nature of the global unfolding opening transitions that account for class *c* residues, we hypothesized that their PFs are similarly affected by the removal of cAMP. Indeed, this hypothesis on the concerted response of class *c* residues to cAMP release is confirmed by the observation that the $\Delta \log_{10} PF$ values reported in Fig. 2*d* for class *c* amino acids are well clustered around a value of 2.0. Their standard deviation is only 0.3, which is comparable to the error already implicit in the intrinsic exchange rates used for the PF computation (39, 40). The consistent two-order of magnitude reduction in PF values observed upon cAMP dialysis is also in agreement with the decrease in the $\Delta G_{\text{unfolding}}$ independently revealed by urea denaturation after stripping cAMP (14), thus further corroborating that the exchange of class *c* residues relies on global unfolding events.

''Three-Shell'' Model for the Intramolecular cAMP-Dependent Signaling Networks. The different results discussed above based on the cAMP-induced variations in H/H–H/D PFs and chemical shifts are accounted for here in a unified manner through a three-shell allosteric model, which we propose for the intramolecular cAMP-dependent signaling networks of CBD-A. In the context of this

model, the ensemble of contacts that radiate out from the PBC and the contiguous strands propagating the cAMP signal beyond the cAMP-binding site will be collectively referred to here as the "primary shell" of cAMP-dependent interactions (Fig. 4*a*). The 2D contact map shown in Fig. 3*c* reveals that all of the sites that are most sensitive to the cAMP-dependent long-range effects as judged based on the compounded chemical shift variations (i.e., "hot spots," Fig. 3*b*) are accounted for by the primary shell of contacts radiating directly from the PBC. Two of these sites, i.e., the α-B′ helix and the C-helix, fall within regions that are in direct contact with the C-subunit and are consistent with the N-terminal capping of the α-B′ helix by the cAMP phosphate (6) and with the E200/R241 electrostatic switch (9) (Fig. 4*a*) and/or the hydrophobic hinge (11, 12). However, some key sites that are clearly affected by cAMP based on chemical-shift mapping are not involved in direct contacts with the C-subunit. Even though these cAMP-dependent interactions within the primary shell do not lead directly to C-binding sites, they still have the potential to contribute to the control of C recognition by functioning as relay points that propagate the cAMP signal beyond the first "wave" of contacts. These sites include the conserved D170 and I163, located at the N terminus of the β_3 strand and the C terminus of the β_2 strand, respectively (Fig. 4*a*). The major effect of cAMP on the D170 region is accounted for by a salt bridge between its carboxylate and the guanidinium group of R209, which also anchors the equatorial exocyclic oxygen of the cAMP phosphate (6). In addition, the guanidinium of R209 is hydrogen-bonded to the backbone carbonyl oxygen of N171 (Fig. 4*a*), whereas the N171 amide hydrogen-bonds the carboxylate of D170 (Fig. 4*d*). The backbone carbonyl oxygen of D170 is in turn hydrogen-bonded with the backbone amide of R226 at the N terminus of the B-helix, which is part of a second shell of contacts that relay the cAMP signal (Fig. 4 *b* and *d*). Specifically, the enhanced solvent exposure observed for D170 in the absence of cAMP (Fig. 2 *b* and *e*) is consistent with the increased flexibility required for the B-helix hinge motions necessary to bind the C-subunit (Fig. 4*e*).

The D170-relayed signaling pathway also explains why the D170A mutant of R is nonallosteric and is able to inhibit the C-subunit stoichiometrically even in the presence of cAMP (17). However, because it is known that C binding causes a global reorganization of the α-subdomain (7), additional intramolecular signaling pathways should be considered to explain how conformational plasticity is introduced at multiple sites within the α/β-subdomain interface by the release of cAMP. For instance, another possible signaling pathway might be controlled by I163, which is the other major cAMP-dependent locus revealed through N_z spectroscopy. I163 is in close contact with the methylenes of the R209 side chain and together with V162 is part of a previously identified conserved hydrophobic layer at the C terminus of the β_2 strand, which has evolved to protect the cAMP phosphate from attack by phosphodiesterases (1) (Fig. 4*b*).

Both V162 and I163 also belong to an extended core of class *c* residues that in the presence of cAMP exchange concertedly through transient global unfolding events and include several other amides with $\log PF_{cAMP\text{-}Bound} > 6$ mainly clustered in the inner strands of the β-sandwich (strands 3, 4 and 7, 8) (Fig. 2*a*). It is, therefore, possible that the local perturbation at the conserved V162/I163 sites initially caused by cAMP removal has a more extensive concerted effect that contributes to collectively perturbing the whole set of class *c* interactions and promotes partial but global unfolding for the other class *c* residues as confirmed by Fig. 2*d*, including amino acids at the α/β-subdomain interface, such as F172, V174, I224, and W222 (Fig. 4*c*, tertiary shell). Although other loci may also contribute to promoting partial global unfolding in a cAMP-dependent manner, the I163 relay site is conveniently activated by cAMP through interactions with the same highly conserved PBC residue that activates D170, i.e., R209 which, in turn, contacts the cyclic phosphate (SI Table 1) defining a pervasive allosteric network nucleated by cAMP binding (Fig. 4). Conversely, release of cAMP breaks this extended circuitry relayed by the sites centered at I163 and D170 and uncouples the α- and β-subdomains from each other. In addition, the loop between I163 and D170 includes other key residues, i.e., the highly conserved G166 (1), which is hydrogen-bonded to the carbonyl of R209 (SI Table 1), and G169, which is critical for the cAMP-mediated activation of PKA as indicated by genetic screening (18), further reaffirming the pivotal role of this turn region for allostery.

We predict that the proposed three-shell model will be relevant not only for the control of the kinase activity in the PKA system but also for other homologous CBDs coupled to diverse functions. Furthermore, this work demonstrates how a small ligand such as cAMP can allosterically alter protein–protein interactions, thus opening additional perspectives in drug design.

Materials and Methods

Sample Preparation. The R-subunit of PKA (residues 119–244) was expressed and purified based on known protocols as described (8). The ^{15}N-labeled protein was expressed in 2 liters of ^{15}N-enriched minimal media (Spectra 9; Spectra Stable Isotopes, Columbia, MD). For all NMR samples the purified protein was dissolved in 50 mM Mes (pH 6.5)/100 mM NaCl/0.02% NaN_3.

NMR Spectroscopy. An AV 700 spectrometer (Bruker, Billerica, MA) equipped with a cryo-probe was used for the acquisition of all NMR data. The probe temperature was set at 306 K, resulting in well dispersed heteronuclear single-quantum coherence (HSQC) cross-peaks. The assignment of cAMP-bound RIα (119–244) has been deposited in the BioMagResBank (BMRB) database with accession number 6984. The N_z exchange experiments (42–44) were run with an N_z mixing period of 230 ms by using a sample that contained detectable amounts of both free and cAMP-bound RIα (residues 119–244). However, because the pure cAMP-free state of RIα (residues 119–244) is only poorly stable in solution under the experimental conditions used, the cAMP-induced variations in hydrogen exchange rates were measured by perturbing the binding equilibrium just slightly, i.e., by dialyzing out the excess free-cAMP under native conditions so that only minor populations of the cAMP-free state would coexist in dynamic equilibrium with the bound form of the protein (45). The low concentration of the free state and the dynamic exchange of the cAMP ligand between the free and bound proteins ensures the stability of these samples during the measurement of the hydrogen exchange rates (45). The H/D exchange was monitored in real time by a series of HSQC spectra (46, 47). The first 30 HSQC experiments acquired after exposure to D_2O accumulated only two scans per serial file, minimizing the total acquisition time per HSQC to ≈10 min and consequently leading to a better sampling of the fast decaying amides. For the subsequent decay the number of scans was doubled to four, and 44 additional HSQC spectra were recorded. The H/H exchange rates between water and the backbone amide protons were measured by using a CLEANEX-PM-FHSQC pulse sequence (48–51) with mixing times of 5, 10, 30, 40, 60, and 80 ms. Further details are available in *SI Materials and Methods*.

This work was supported by the Canadian Institutes of Health Research, McMaster University, the Canada Foundation for Innovation (G.M.), and National Institutes of Health Grant GM34921 (to S.S.T.). G.M. was supported by the Heart and Stroke Foundation of Canada's Maureen Andrew New Investigator Award.

1. Berman HM, Ten Eyck LF, Goodsell DS, Haste NM, Kornev A, Taylor SS (2005) *Proc Natl Acad Sci USA* 102:45–50.
2. Krebs EG (1993) *Biosci Rep* 13:127–142.
3. Hanks SK, Hunter T (1995) *FASEB J* 9:576–596.

4. Beebe SJ, Corbin JD (1986) *The Enzymes: Control by Phosphorylation* (Academic, New York), pp 43–111.
5. Johnson DA, Akamine P, Radzio-Andzelm E, Madhusudan M, Taylor SS (2001) *Chem Rev* 101:2243–2270.
6. Su Y, Dostmann WR, Herberg FW, Durick K, Xuong NH, Ten Eyck L, Taylor SS, Varughese KI (1995) *Science* 269:807–813.
7. Kim C, Xuong NH, Taylor SS (2005) *Science* 307:690–696.
8. Hamuro Y, Anand GS, Kim JS, Juliano C, Stranz DD, Taylor SS, Woods VL, Jr (2004) *J Mol Biol* 340:1185–1196.
9. Vigil D, Lin JH, Sotriffer CA, Pennypacker JK, McCammon JA, Taylor SS (2006) *Protein Sci* 15:113–121.
10. Gullingsrud J, Kim C, Taylor SS, McCammon JA (2006) *Structure (London)* 14:141–149.
11. Rehmann H, Prakash B, Wolf E, Rueppel A, de Rooij J, Bos JL, Wittinghofer A (2003) *Nat Struct Biol* 10:26–32.
12. Hahnefeld C, Moll D, Goette M, Herberg FW (2005) *Biol Chem* 386:623–631.
13. Anand GS, Hughes CA, Jones JM, Taylor SS, Komives EA (2002) *J Mol Biol* 323:377–386.
14. Canaves JM, Leon DA, Taylor SS (2000) *Biochemistry* 39:15022–15031.
15. Leon DA, Canaves JM, Taylor SS (2000) *Biochemistry* 39:5662–5671.
16. Li F, Gangal M, Jones JM, Deich J, Lovett KE, Taylor SS, Johnson DA (2000) *Biochemistry* 39:15626–15632.
17. Gibson RM, Ji-Buechler Y, Taylor SS (1997) *J Biol Chem* 272:16343–16350.
18. McKnight GS, Clegg CH, Uhler MD, Chrivia JC, Cadd GG, Correll LA, Otten AD (1988) *Recent Prog Horm Res* 44:307–335.
19. Gorman KA, Steinberg RA (1994) *Somat Cell Mol Genet* 20:301–311.
20. Chen S, Vojtechovsky J, Parkinson GN, Ebright RH, Berman HM (2001) *J Mol Biol* 314:63–74.
21. Chen S, Gunasekera A, Zhang X, Kunkel TA, Ebright RH, Berman HM (2001) *J Mol Biol* 314:75–82.
22. Dai J, Lin SH, Kemmis C, Chin AJ, Lee JC (2004) *Biochemistry* 43:8901–8910.
23. Dong A, Malecki JM, Lee L, Carpenter JF, Lee JC (2002) *Biochemistry* 41:6660–6667.
24. Gekko K, Obu N, Li J, Lee JC (2004) *Biochemistry* 43:3844–3852.
25. Lawson CL, Swigon D, Murakami KS, Darst SA, Berman HM, Ebright RH (2004) *Curr Opin Struct Biol* 14:10–20.
26. Li J, Cheng X, Lee JC (2002) *Biochemistry* 41:14771–14778.
27. Lin SH, Lee JC (2002) *Biochemistry* 41:11857–11867.
28. Napoli AA, Lawson CL, Ebright RH, Berman HM (2006) *J Mol Biol* 357:173–183.
29. Parkinson GN, Wu Y, Fan P, Kohn J, Baum J, Berman HM (1994) *Biopolymers* 34:403–414.
30. Passner JM, Schultz SC, Steitz TA (2000) *J Mol Biol* 304:847–859.
31. Weber IT, Steitz TA (1987) *J Mol Biol* 198:311–326.
32. Matulef K, Zagotta WN (2003) *Annu Rev Cell Dev Biol* 19:23–44.
33. Clayton GM, Silverman WR, Heginbotham L, Morais-Cabral JH (2004) *Cell* 119:615–627.
34. Loh SN, Prehoda KE, Wang J, Markley JL (1993) *Biochemistry* 32:11022–11028.
35. Meisner WK, Sosnick TR (2004) *Proc Natl Acad Sci USA* 101:15639–15644.
36. Bai Y, Englander JJ, Mayne L, Milne JS, Englander SW (1995) *Methods Enzymol* 259:344–356.
37. Gavina JL, Das R, Britz-McKibbin P (2006) *Electrophoresis* 27:4196–4204.
38. Dempsey CE (2001) *Progr NMR Spect* 39:135–170.
39. Zhang YZ (1995) PhD thesis (Univ of Pennsylvania, Philadelphia).
40. Bai Y, Milne JS, Mayne L, Englander SW (1993) *Proteins Struct Funct Genet* 17:75–86.
41. Koradi R, Berman HM, Wüthrich K (1996) *J Mol Graphics* 14:51–55.
42. Farrow NA, Zhang O, Forman-Kay JD, Kay LE (1994) *J Biomol NMR* 4:727–734.
43. Vialle-Printems C, van Heijenoort C, Guittet E (2000) *J Magn Reson* 142:276–279.
44. Rodriguez JC, Jennings PA, Melacini G (2004) *J Biomol NMR* 30:155–161.
45. Das R, Abu-Abed M, Melacini G (2006) *J Am Chem Soc* 128:8406–8407.
46. Palmer AG, Cavanagh J, Wright PE, Rance M (1991) *J Magn Reson* 93:151–170.
47. Kay LE, Keifer P, Saarinen T (1992) *J Am Chem Soc* 114:10663–10665.
48. Hwang TL, van Zijl PCM, Mori S (1998) *J Biomol NMR* 11:221–226.
49. Grzesiek S, Bax A (1993) *J Biomol NMR* 3:627–638.
50. Kriwacki RW, Hill RB, Flanagan JM, Caradonna JP, Prestegard JH (1993) *J Am Chem Soc* 115:8907–8911.
51. Huang H, Melacini G (2006) *Anal Chim Acta* 564:1–9.